ELSEVIER

International Journal of Mass Spectrometry 190/191 (1999) 113–127

International Journal of Mass Spectrometry

Some features of "unstable" trajectories of ions within hyperboloid mass spectrometers and the problem of charged particle analysis

Ernst P. Sheretov*, Tatiana B. Karnav, Alexander V. Brykov

Department of Physics, Ryazan State Radio Technical University, Ryazan 391000, Russia

Received 22 September 1998; accepted 9 February 1999

Abstract

In this article we discuss some features of unstable ion trajectories in hyperboloid mass spectrometers. It is shown that some unstable ions may have absolutely convergent trajectories (base trajectories). As a result, the required sorting time is greatly increased, and the maximum allowed resolution and analysis rate are decreased. Factors influencing the base trajectories (periodic fluctuation of rf signal shape; mass scanning rate and a scan function shape; ion/molecule interactions of the residual gas in a vacuum chamber) are investigated. The results of experimental studies that exhibit rather surprising results of the theory are presented. (Int J Mass Spectrom 190/191 (1999) 113–127) © 1999 Elsevier Science B.V.

Keywords: Quadrupole ion trap; Mass spectrometry; Quadrupole ion trap mass spectrometry; Mass filter; Hill equation

1. Introduction

Hyperboloid mass spectrometers are devices utilizing oscillating electric fields for ion containment in two or three dimensions. In the general case the working surfaces of electrode systems are one-sheet hyperboloid or parted hyperboloid. When mass spectrometry first employed electrodynamic fields there were only two types of electrode systems: the linear quadrupole mass filter and the axially symmetric ion trap [1]. A diversity of different electrode systems has been described since that time. This prompts us to suggest that the mass spectrometry community use a general title for such mass spectrometers: hyperboloid mass spectrometers (HMS). The theoretical basis for the operation of these devices is the theory of differential equations of second order with periodic coefficients developed in detail at the end of the last century. Two types of equations are important for hyperboloid mass spectrometry: the Hill equation and its special case—the Mathieu equation.

The development of hyperboloid mass spectrometers was accompanied by spectacular achievements in the theory of such devices. The dynamics of this thrilling process can be retraced in the fundamental works of Paul and Steinwedel [2], Dawson and Whetten [3,4], March and Todd [5,6,7], and other scientists who provided leadership in this technique of dynamic mass spectrometry.

The principle of independence of ion oscillations along the different coordinate axes is implied in the classical variant of HMS. Such a mode of operation is

* Corresponding author. E-mail: sheretov@eac.ryazan.su

Dedicated to J.F.J. Todd and R.E. March in recognition of their original contributions to quadrupole ion trap mass spectrometry.

PII S1387-3806(99)00027-5

called a linear mode. To describe this mode it is sufficient to analyze solutions of the canonical Hill or Mathieu equation [8].

In the present article some features of the divergent solutions of the Hill equation that determine trajectories of the respective ions are discussed in terms of the linear theory. Two major processes define the analytical capability of HMS: the confinement of the needed ions within the dynamic three-dimensional field (this process determines the sensitivity of a device, in general), and a process of ion sorting (when unwanted ions collide with the analyzer electrodes). The second process is concerned with trajectories of unstable ions and defines the resolution that can be achieved with a mass spectrometer.

It is commonly accepted that unstable ions have trajectories with a continuously growing amplitude and, therefore, in order to achieve the required resolution for ions with different values of mass to charge ratio (m/z) it is sufficient to set the respective sorting time. But, we will show here that some ions, with working points that lie within unstable regions of the general stability diagram, may have absolutely converging trajectories (base trajectories). Thus, the time of sorting of the ions and removing them from an analyzer is sharply increased and in principle tends to infinity. These ions can limit the relative sensitivity of HMS, deteriorate mass peak shapes, and increase sorting time which, in turn, limits the maximum analysis speed.

2. Base solutions

Different shapes of rf signals, such as square or sine waves, that can be applied to electrodes of hyperboloid mass spectrometers have been used increasingly. Therefore, we study here some features of the Hill equation as the general equation describing trajectories of the charged particles. Our focus here is on the linear theory of HMS, which does not include the field distortions and which implies the principle of independence of ion oscillations along the different axes. This allows us to confine ourselves to solving a one-dimensional problem.

The Hill equation is

$$\ddot{y}(t) + \Psi(t)y(t) = 0 \tag{1}$$

where $\Psi(t)$ is a periodic function of period t_p. Let us consider $y_1(t)$ and $y_2(t)$ as two particular independent solutions of Eq. (1); y_0, $\dot{y}_0$, and t_0—the initial coordinate, velocity, and phase; α_1 and α_2, β_1 and β_2—elements of the transformation matrix of partial solutions (Floquet's coefficients [8]):

$$\begin{bmatrix} y_1(t+t_p) \\ y_2(t+t_p) \end{bmatrix} = \begin{bmatrix} \alpha_1 & \alpha_2 \\ \beta_1 & \beta_2 \end{bmatrix} \times \begin{bmatrix} y_1(t) \\ y_2(t) \end{bmatrix} \tag{2}$$

Then we have:

$$\gamma_0 y(t) = y_0[\dot{y}_2(t_0)y_1(t) - \dot{y}_1(t_0)y_2(t)] + \dot{y}_0[y_1(t_0)y_2(t) - y_2(t_0)y_1(t)] \tag{3}$$

$$\gamma_0 y(t+t_p) = y_0\begin{bmatrix} \dot{y}_2(t_0)\langle\alpha_1 y_1(t) + \alpha_2 y_2(t)\rangle \\ -\dot{y}_1(t_0)\langle\beta_1 y_1(t) + \beta_2 y_2(t)\rangle \end{bmatrix} + \dot{y}_0\begin{bmatrix} y_1(t_0)\langle\beta_1 y_1(t) + \beta_2 y_2(t)\rangle \\ -y_2(t_0)\langle\alpha_1 y_1(t) + \alpha_2 y_2(t)\rangle \end{bmatrix} \tag{4}$$

where γ_0 is the Wronskian determinant:

$$\gamma_0 = \dot{y}_2(t)y_1(t) - \dot{y}_1(t)y_2(t) \tag{5}$$

Now we find conditions under which the following expression is correct:

$$y(t+t_p) = K_0 y(t) \tag{6}$$

where K_0 is a constant.

From Eqs. (2)–(5) we obtain the following system:

$$K_{0_{1,2}} = \beta_0 \pm (\beta_0^2 - 1)^{1/2} \tag{7a}$$

$$y_0^2[(\beta_2 - \alpha_1)\dot{y}_2(t_0)\dot{y}_1(t_0) + \beta_1\dot{y}_1^2(t_0) - \alpha_2\dot{y}_2^2(t_0)] + \dot{y}_0^2[(\beta_2 - \alpha_1)y_2(t_0)y_1(t_0) + \beta_1 y_1^2(t_0) - \alpha_2 y_2^2(t_0)] - 2y_0\dot{y}_0\begin{bmatrix} (\beta_2 - \alpha_1)\langle\dot{y}_2(t_0)y_1(t_0) + \dot{y}_1(t_0)y_2(t_0)\rangle/2 \\ +\beta_1\dot{y}_1(t_0)y_1(t_0) - \alpha_2\dot{y}_2(t_0)y_2(t_0) \end{bmatrix} = 0 \tag{7b}$$

where $\beta_0 = (\alpha_1 + \beta_2)/2$, the stability parameter well known in theory [1]. If $\beta_0^2 > 1$ then we have unstable solutions of Eq. (1) and if $\beta_0^2 < 1$, solutions are stable. Solutions are unstable if the amplitude of motion, $y(t)$

unrestrictedly increases with time; solutions are stable when the amplitude is limited in time. The function $\Psi(t)$ has some parameters. For example, for the canonical form of the Mathieu equation $\Psi(t) = a - 2q\cos(2t)$ the parameters are coefficients a and q that define the stability diagram. The boundaries of the diagram correspond to $\beta_0^2 = 1$. The stability diagram is fundamental for the theory of HMS.

Substitution of the obtained expression for K_0 into Eq. (6) yields

$$\frac{y(t + t_p)}{y(t)} = \beta_0 \pm (\beta_0^2 - 1)^{1/2} \tag{8}$$

Let us carefully investigate the meaning of this equation. Now, if $\beta_0^2 \geq 1$, then the solution is unstable and the right part of Eq. (8) is real. If $\beta_0 > 1$, then for the plus sign in (8) we have determined that the right part is greater than 1. This means that a coordinate of the charged particle is continuously increased from one period to another and we have a growing solution. If $\beta_0 > 1$, then for the minus sign in (8) K_{0_2} is always less than 1 and a coordinate continuously decreases and converges to zero from period to period. Thus, we come to an important conclusion: Eq. (8) describes two types of unstable solutions. One solution is continuously divergent [the plus sign in Eq. (8)] and the other is continuously convergent [the minus sign in Eq. (8)]. It can be seen that in the unstable region for which $\beta_0 < -1$, the plus sign in Eq. (8) corresponds to a continuously convergent solution and the minus sign corresponds to a continuously divergent solution. It should be noted, however, that in the last case the general solution changes its sign from period to period, and the respective trajectory has the character of oscillatory movement with a growing amplitude. Let us call continuously convergent unstable solutions base solutions and the corresponding trajectories of ions base trajectories.

It is easy to note from Eq. (8) that the rate of convergence of the base solutions and the rate of growth of continuously divergent solutions are determined by the parameter β_0 only. At those boundaries of the diagram where $\beta_0^2 = 1$, the rate converges to zero. If $|\beta_0|$ is increased, then the rate of growth of continuously divergent solutions and the rate of convergence of the base trajectories [which satisfy Eqs. (6), (7b), and (8)] are increased. At the boundaries of the diagram these solutions degenerate to one solution for which

$$\frac{y(t + t_p)}{y(t)} = \pm 1 \tag{9}$$

Here the rate of convergence of the base solutions is equal to zero. Let us call such solutions the equilibrium solutions and the corresponding trajectories of ions equilibrium trajectories. We see two signs in Eq. (9). This means that there are two types of such solutions. For the plus sign in Eq. (9) we obtain one solution for which the coordinate is repeated over the period; for the minus sign we have the other solution for which the coordinate changes its sign only.

We obtain initial conditions under which these trajectories can be achieved from Eq. (7b). This equation describes two lines lying on the phase plane, and intersecting the origin. One line corresponds to the base solution, and the other corresponds to a continuously divergent solution. The line corresponding to the base solution coincides with the line of the continuously divergent solution.

Thus, trajectories of ions, working points of which lie in the unstable region of the stability diagram, can absolutely converge and the time of flight of ions within the analyzer is infinite. This means that such unstable particles cannot be removed from the analyzer.

It should be noted that Eqs. (6), (8), and (9) are also valid for velocities of ions. For example, if the coordinate of an ion, the trajectory of which is a base trajectory, is decreased, then the velocity of the ion is decreased also, and converges to zero in time. Finally, ions are focused to the center.

3. Some features of “regular” unstable solutions of the Hill equation

Our task here is to study some features of regular unstable solutions, for which Eqs. (6), (7b), and (8) are not true.

If we have $t = t_0$, we find the following system from Eqs. (2), (3), and (4):

$$\gamma\dot{y}(t_0 + t_p) = \Psi_1 y_0 + \Psi_2 \dot{y}_0$$
$$\gamma y(t_0 + t_p) = \Psi_3 y_0 + \Psi_4 \dot{y}_0 \tag{10}$$

where Ψ_i are functions of t_0 (initial phase).

Now we can obtain

$$\Delta(n+1) = \frac{\Psi_1 + \Delta(n)\Psi_2}{\Psi_3 + \Delta(n)\Psi_4} \tag{11}$$

where $\Delta(n) = \dot{y}_0(n)/y_0(n)$ is the slope of the line lying on the phase plane on which the ion characteristic point is currently located at the beginning of the nth period of function $\Psi(t)$; and $\Delta(n+1)$ at the end of that period.

We can see from (10) that coefficients Ψ_i are coefficients of the transformation matrix for the general solution of the Hill equation (α_1, α_2, β_1, and β_2 are transformation coefficients of partial solutions for this equation). These coefficients can be easily transformed into each other. Practically, it is more convenient to use coefficients Ψ_i for a complicated function $\Psi(t)$ in Eq. (1) [if $\Psi(t)$ is a square function, for instance]. Coefficients α_i and β_i can be used if analytic expressions for $y_1(t)$ and $y_2(t)$ are known (for example, in the case of the Mathieu equation [8]).

It can be shown that the following expressions are true:

$$2\beta_0 = \alpha_1 + \beta_2 = \Psi_2 + \Psi_3$$
$$\alpha_2\beta_1 - \beta_2\alpha_1 = \Psi_2\Psi_3 - \Psi_1\Psi_4 = 1 \tag{12}$$

Expression (11) and Ψ_i show how the location of the working line of the ion on the phase plane is changed from period to period. It can be seen that for $\Delta(n)$ there is a stationary value Δ_{00} that is constant from period to period t_p. From (11) we can obtain the following equation for two values $\Delta_{00_{1,2}}$:

$$\Delta_{00_{1,2}} = \frac{-\Psi_3 + \beta_0 \pm (\beta_0^2 - 1)^{1/2}}{\Psi_4} \tag{13}$$

When we substitute Eq. (13) into Eq. (10) and apply $y_0 = y(n)$ and $\dot{y}_0 = \dot{y}(n)$, we obtain an expression identical to Eq. (8):

$$\frac{y(n+1)}{y(n)} = \beta_0 \pm (\beta_0^2 - 1)^{1/2} \tag{14}$$

This means that the base solution has an interesting feature: the characteristic point of an ion on the phase plane returns to the same line over one period. This feature, of course, is also specific for a continuously divergent solution. Thus, we should define unstable solutions (and trajectories also), which satisfy Eqs. (6), (7b), and (8), as stationary.

In the case when $\Delta(n)$ is close to Δ_{00}, the change of remainder $\Delta p = \Delta(n) - \Delta_{00}$ over the period may be estimated as:

$$\Delta p \cong \Delta p_0 \exp\left(-2\,\frac{\pm(\beta_0^2 - 1)^{1/2}}{\beta_0 \pm (\beta_0^2 - 1)^{1/2}}\right) \tag{15}$$

Now, if $\beta_0 > 1$ then for the plus sign in Eq. (15), Δp is decreased in time (over the next period). This means that $\Delta(n)$ converges to Δ_{00} in time (from period to period). For the minus sign in Eq. (15) Δp is increased in time.

If $\beta_0 < -1$ the situation changes: under the upper sign in Eq. (15) Δp is increased and for the lower sign Δp is decreased and converges to zero. This indicates that ordinary unstable solutions, for which the initial value of the working line slope Δ_0 is different from Δ_{00}, converges to one stationary solution in time and goes away from the other. The first stationary solution is called steady stationary solution (SSS) and the second—unsteady stationary solution (USS). We have mentioned above that the ordinary solutions ($\Delta_0 \neq \Delta_{00}$) converge to the SSS and go away from the USS. This means that trajectories of the unstable particles become similar with time and for a given working point at the stability diagram all unstable particles make synchronous oscillatory movements. It is easy to demonstrate that in the case of a square rf signal all particles pass their extreme points at the same time. Thus, the base solutions of the Hill equation are the unsteady stationary solutions. The

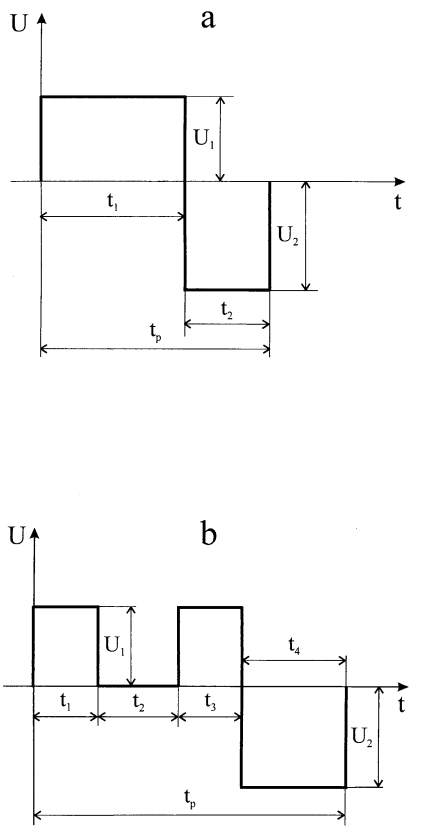

Fig. 1. Waveforms of the rf signals. (a) A square wave signal; $t_1 = t_2$ for the meander; (b) the EC signal ($t_1 = t_3$); t_p is the period of the signal.

continuously divergent solutions are the steady stationary solutions.

In the case when a square wave rf signal (Fig. 1) is applied to the electrode system of the analyzer we obtain a simple equation for the extreme characteristic solution [9,10]:

$$y^2_{\text{extr}}(n) = c_1 + c_2 \exp(2\omega n) + c_3 \exp(-2\omega n) \tag{16a}$$

where

$$c_1 = \frac{1}{2}\left[y_0^2 + \frac{\dot{y}_0^2}{a_1^2} - \frac{1}{a_1^2} b_0^2 - d_0^2\right]$$

$$c_2 = \frac{1}{4}\left[(y_0 + d_0)^2 + \frac{1}{a_1^2}(\dot{y}_0 + b_0)^2\right] \tag{16b}$$

$$c_3 = \frac{1}{4}\left[(y_0 - d_0)^2 + \frac{1}{a_1^2}(\dot{y}_0 - b_0)^2\right]$$

n—time (number of periods);

$$b_0 = \frac{y_0\Psi_1 + \dot{y}_0[\Psi_2 - \beta_0]}{(\beta_0^2 - 1)^{1/2}}$$

$$d_0 = \frac{\dot{y}_0\Psi_4 + y_0[\Psi_3 - \beta_0]}{(\beta_0^2 - 1)^{1/2}} \tag{16c}$$

$$a_1^2 = \frac{2ZU_1\eta t_p^2}{m(1 + n_0 + p_0)y_a^2}$$

$$a_2^2 = \frac{2ZU_2\eta t_p^2}{m(1 + n_0 + p_0)y_a^2}$$

where a_1 and a_2 are pulse coordinates that define the stability diagram; Z and m are charge and mass of an ion, respectively; U_1 is the amplitude of the positive pulse (focusing pulse); U_2 is the amplitude of the negative pulse (defocusing pulse); t_p is the period of the rf signal; n_0, p_0, and η are geometrical parameters of the electrode system: $n_0 = x_a^2/y_a^2$; $p_0 = x_a^2/z_a^2$; x_a, y_a, z_a are distances between the electrode system center and electrodes along the corresponding axes; $\eta = 1$ for the x coordinate, $\eta = 1 + p_0$ for the y coordinate, and $\eta = p_0$ for the z coordinate. For the quadrupole mass filter $p_0 = 0$; for the axisymmetrical ion trap $p_0 = 1$.

The function (16a) defines extreme values of the general solution at the nth period and can be interpreted as an envelope curve.

It follows from (16a) that for the SSS the condition $c_3 = 0$ remains true and for the base solution condition $c_2 = 0$ remains true; $c_1 = 0$ in both cases. For the ordinary solutions $c_2 \neq 0$ and $c_3 \neq 0$. The amplitude of an ion trajectory can be either increased at once after injection or decreased (compressed) and then increased depending on the ratio between c_1 and c_2. Compressed trajectories appear when $c_3 \geq c_2$.

Compression of an unstable ion beam is very unfavorable for effective sorting, because it increases the required sorting time of ions. However, in our opinion, compression of ion trajectories demonstrates

attractive prospects in terms of the ion trapping and development of new analytical principles.

The time of ion trapping in the trap volume, n_{trap}, is determined from Eq. (16a) when $y^2_{extr}(n_{trap}) = 1$. If $c_2 = 0$ then the trapping time approaches infinity ("base" trajectories). In this case "phase," "energy," and "space" windows for the trapped particles tend to zero. For finite values of the trapping time, these windows expand, which allows practical use of this injection technique.

It can be shown that from (16a) we can derive an equation similar to (8):

$$\frac{y_{extr}(n+1)}{y_{extr}(n)} = \beta_0 \pm (\beta_0^2 - 1)^{1/2} \tag{17}$$

When the working point of an ion lies on the $\beta_0^2 = 1$ boundary of the stability diagram then the expression for $y^2_{extr}(n)$ is given by:

$$y^2_{extr}(n) = \{y_0 + [y_0(\Psi_3 - \beta_0) + \dot{y}_0\Psi_4]n\}^2 + \frac{1}{a_1^2}\{\dot{y}_0 + [y_0\Psi_1 + \dot{y}_0(\Psi_2 - \beta_0)]n\}^2 \tag{18}$$

In this case for the equilibrium solution we have

$$K_{0_{1,2}} = \pm 1$$

It follows from (18) that the slope of the working line on the phase plane should be defined as:

$$\frac{\dot{y}_0}{y_0} = -\frac{\Psi_3 - \beta_0}{\Psi_4} = -\frac{\Psi_1}{\Psi_2 - \beta_0} \tag{19}$$

Then the maximum deviation of an ion from the origin does not depend on n and can be found from:

$$y^2_{extr} = y_0^2 + \frac{\dot{y}_0^2}{a_1^2} \tag{20}$$

Such particles can oscillate at some distance from the origin (their coordinates are greater then zero) or in the vicinity of the origin with the same amplitude.

In the case where particles are injected into the rf field during the optimal phase of the first kind (the middle of the focusing pulse—see Fig. 1) it can be shown that $\Psi_2 = \Psi_3 = \beta_0$ and for the $\beta_0^2 = 1$ boundary $\Psi_1\Psi_4 = 0$. This means that on some boundaries $\Psi_1 = 0$ and $\Psi_4 \neq 0$, and on the others $\Psi_4 = 0$ and $\Psi_1 \neq 0$. Thus, we call the former Ψ_1 boundaries and the latter Ψ_4 boundaries. Now, we rewrite Eq. (18) in the following way:

$$y^2_{extr}(n) = \{y_0 + \dot{y}_0\Psi_4 n\}^2 + \frac{1}{a_1^2}\{\dot{y}_0 + y_0\Psi_1 n\}^2 \tag{21}$$

We can see from this equation that on the Ψ_1 boundary for injected ions with zero velocity:

$$y^2_{extr}(n)|_{\Psi_1=0} = y_0^2 \tag{22}$$

i.e. oscillation amplitude is constant; on the Ψ_4 boundary:

$$y^2_{extr}(n)|_{\Psi_4=0} = y_0^2\left[1 + \frac{\Psi_1^2 n^2}{a_1^2}\right] \tag{23}$$

Otherwise, on the Ψ_1 boundary for injected ions with zero coordinate but finite velocity, $\dot{y}_0$,

$$y^2_{extr}(n)|_{\Psi_1=0} = \frac{\dot{y}_0^2}{a_1^2}[1 + a_1^2\Psi_4^2 n^2] \tag{24}$$

i.e. the oscillation amplitude increases in time; and on the Ψ_4 boundary:

$$y^2_{extr}(n)|_{\Psi_4=0} = \frac{\dot{y}_0^2}{a_1^2} \tag{25}$$

i.e. the oscillation amplitude is constant.

The dependence of the z coordinate of an ion as a function of sorting time is demonstrated in Fig. 2 (the trajectory is close to the base one). The working point of the ion is located in the unstable region close to the upper apex of the first stability zone for the ion trap with the square wave rf signal with $t_1 = t_2$ meander [Fig. 1(a)]. The pulse coordinates for the axially symmetric ion trap can be described as

$$a_{1r}^2 = \frac{2ZU_1t_p^2}{m(2+n_0)d^2};\ a_{2r}^2 = \frac{2ZU_2t_p^2}{m(2+n_0)d^2};\ n_0 = r_a^2/d^2$$

where r_a is the minimum distance between the electrode system center and the ring electrode, and d is the

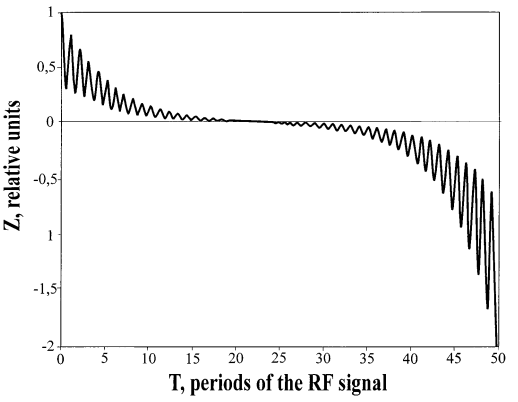

Fig. 2. Temporary converging trajectory of an ion within the axially symmetric ion trap in the case when the rf signal meander is applied to the electrodes; initial coordinate $z_0 = 1$; initial velocity $\dot{z}_0 = -0.3016$; initial phase $T_0 = T_{BS} - 1.5 \times 10^{-6} = 0.770014$; $a_1 = 3.579669$, $a_2 = 2.498629$; $\beta_{0z} = 1.01824$; where T, T_0, T_{BS} are time, initial phase, and initial phase corresponding to the base trajectory, respectively, normalized to an rf period.

minimum distance between the electrode system center and one endcap electrode. Coordinates r and z are normalized to the characteristic dimension of the electrode system d; normalized velocities are given by

$$\dot{r} = \dot{r}_{\text{real}} \frac{t_p}{d}; \dot{z} = \dot{z}_{\text{real}} \frac{t_p}{d} \tag{26}$$

where $\dot{r}_{\text{real}}$ is the absolute value of ion velocity along the r coordinate; $\dot{z}_{\text{real}}$ is the absolute value of ion velocity along the z coordinate.

It can be seen from Fig. 2 that time of flight of the unstable ion (m/z 28) in the field is 45 periods of the rf field even for a large initial coordinate ($z_0 = 1$) and initial velocity ($\dot{z}_0 = -0.3016$). The entrance (initial) energy of the ion is 1.4 eV; the amplitude U_1 of the positive pulse is 590 V; $t_p = 1.9$ μs; $a_1 = 3.579669$; $d = r_a = 19$ mm.

4. Base solutions of first and second kinds. Lines of absolute focusing

The solutions with initial conditions of the first and second kinds are very important for theory of the HMS. Solutions of the first kind are defined for $\dot{y}_0 = 0$, and solutions of the second for $y_0 = 0$. For example, for the ion trap with an electron beam to form ions and a large amplitude of rf signal applied to electrodes, the initial velocities of the created ions can approximately be taken equal to zero. Under these circumstances we can describe parameters of such a device by using solutions of the Hill equation of the first kind. For the quadrupole mass filter, transverse velocities of the injected ions may greatly exceed thermal velocities, but initial coordinates are small because of small entrance holes. Here, solutions of the equation of the second kind became important.

Conditions under which the base solutions of the first kind and the second kind are possible can be defined from Eq. (7b). It is easy to see that the expression in the first set of brackets is equal to zero for stationary solutions of the first kind; the expression in the second set of brackets is equal to zero for stationary solutions of the second kind.

It can be shown that the condition:

$$\Psi_1 = 0 \tag{27}$$

is true for stationary solutions of the first kind; and the condition:

$$\Psi_4 = 0 \tag{28}$$

is true for stationary solutions of the second kind.

For base solutions [in addition to (27) and (28)] we must allow for the following conditions: for base solutions of the second kind when $\beta_0 > 1$ then $\Psi_3 > 1$; when $\beta_0 < -1$ then $\Psi_3 < -1$. For base solutions of the first kind: when $\beta_0 > 1$ then $\Psi_2 > 1$, and when $\beta_0 < -1$ then $\Psi_2 < -1$.

It can be shown from (12) that these additional conditions contradict each other. This means that in different instability regions (we mean zones with $\beta_0 > 1$ and $\beta_0 < -1$) only different base solutions are possible—of the first kind or the second.

All conditions, (27) and (28) with additional conditions, describe lines of base solutions of both kinds. The location of each line of such a family within the instability zone is defined by the initial phase and by the shape of the function $\Psi(t)$ in Eq. (1). When the additional conditions described are in contrast to conditions (27) and (28), then we do not have any

base solutions in these zones and only the stationary steady solutions are possible there.

The general stability diagram for a given HMS is formed by simultaneous overlapping of zones for the respective coordinates. Here, zones (in which lines of base solutions are possible) overlap each other, and lines of absolute focusing appear.

For one phase these lines are the locus of points that are formed by intersection of lines of base solutions for different coordinate axes. When the working point is located on a line of absolute focusing, then (for the quadrupole mass filter, for example) an ion injected into the field will move along the symmetry axis for some time. Within the ion trap such an ion will focus in the center of electrode system and stop there after a period of time where it will theoretically stay for an indefinite time. This means that the sorting rate of unstable ions is dramatically decreased. These ions are herded in the center of the ion trap at first, and then they are slowly moved to electrodes.

Three types of absolute focusing may appear in the general case: absolute focusing lines of the first, second, and mixed kinds. In the first case, lines are defined by the base solutions of the first kind; in the second case—by base solutions of the second kind; in the third case—by base solutions of both the first and the second kinds. For the quadrupole mass filter, the absolute focusing line of the second kind is important; for the ion trap with injection of ionizing electron beam, the absolute focusing line of the mixed kind is important. For example, when the electron beam is injected along the z coordinate, base solutions of the second kind are important for the r coordinate, and for the z coordinate, the base solutions of the first kind are important.

In Fig. 3 the general stability diagram for the quadrupole mass filter is shown with lines of absolute focusing of the second kind; lines of the mixed kind for axially symmetric ion trap and its stability diagram are shown in Fig. 4. The stability diagrams are plotted using the pulse parameters a_1 and a_2 as coordinate axes for the square wave rf signal (meander).

The trajectory of an ion, the working point of which lies on the line of absolute focusing and labelled 3 in Fig. 4, is demonstrated in Fig. 5 for the

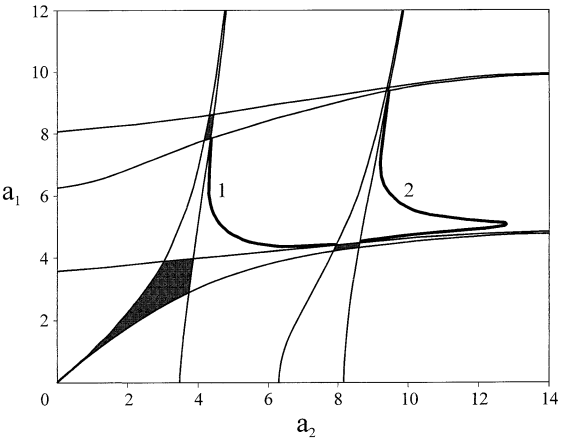

Fig. 3. The general stability diagram in the pulse coordinates a_1 and a_2 for the quadrupole mass filter in the case of meander; 1, 2—absolute focusing lines of the second kind.

axially symmetric ion trap. The conducted calculation showed that in order to get to the center of the analyzer the ion needs only 10 periods of the rf field.

5. Influence of base solutions on sorting of the charged particles in HMS

As we have mentioned above, base trajectories appearing in HMS essentially increase the residence

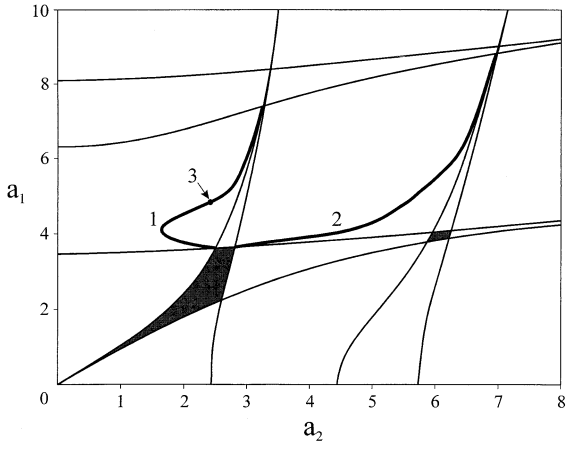

Fig. 4. The general stability diagram in the pulse coordinates a_1 and a_2 for the axially symmetric ion trap in the case of meander; 1, 2—absolute focusing lines of the mixed kind for the r coordinate and of the first kind for the z coordinate; 3—the ion working point, trajectory of which is shown in Fig. 5.

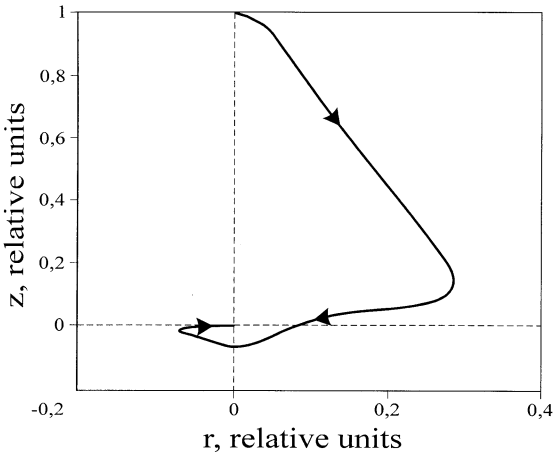

Fig. 5. Trajectory of the ion, working point of which lies on the absolute focusing line of the mixed kind for the axially symmetric ion trap in the case of meander; initial conditions of the first kind for the z coordinate, and initial conditions of the second kind for the r coordinate (the working point is demonstrated in Fig. 4); $a_1 = 3.9693$, $a_2 = 4.1531$, $\beta_{0r} = -1.4664$, $\beta_{0z} = -8.2101$, $T_0 = 0.9$.

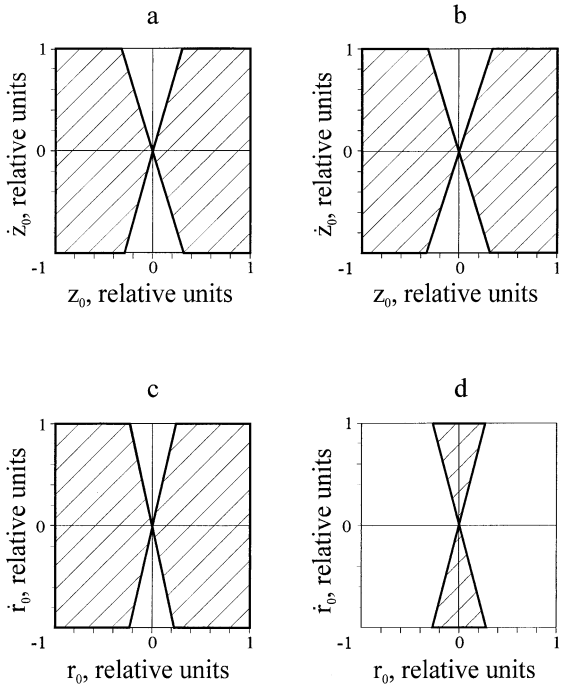

Fig. 6. Zones of base solutions for the axially symmetric ion trap in the case of meander; working points lie close to the apex of the first stability zone; (a), (b) zones of base solutions along the z coordinate: $a_2 = 2.502629$, $a_1 = 3.585399$, $\beta_{0z} = 1.003666$; (c), (d) zones of base solutions along the r coordinate: $a_2 = 2.508805$, $a_1 = 3.594248$, $\beta_{0r} = -1.001748$; (a), (c) the positive (focusing along the r coordinate) pulse; (b), (d) the negative (defocusing along the r coordinate) pulse.

time of unstable particles within the volume of the analyzer. This decreases sorting efficiency, and as a result, affects the mass peak shape. In order to estimate the influence of base trajectories on sorting efficiency we will compare an injection area on the phase plane with so-called zones of "base" solutions.

We have shown above that for a given injection phase of the charged particles there is a line on the phase plane on which all characteristic points of ions with base trajectories lie. Zones of base solutions on the phase plane can be found by varying of initial phase within a possible (or a given) range. If the characteristic point of an ion lies within such a zone, then this ion flies on the base trajectory for an injection phase.

Zones of base solutions are sectors on the phase plane. It is clear that if we inject analyzed ions into the field and their characteristic points lie outside of zones of base solutions, then sorting conditions are favorable.

The shape of zones of base solutions (ZBS) depends on the Ψ_i functions, which in turn, depend on the $\Psi(t)$ function (i.e. on the driving rf signal applied to electrodes). Zones of base solutions for an axially symmetric ion trap are shown in Fig. 6. They are defined for the points located close to the apex of the general stability zone for a square wave rf signal meander. Zones of base solutions are shaded.

We can see that there are some zones that are free from "base" solutions. In order to improve mass peak shape by increasing the sorting efficiency of unstable ions, for ion injection we should make use of zones free from base solutions (ZFBS). It is seen from Fig. 6 that to achieve a high degree of sorting along the r coordinate, the ionizing electron beam should be injected along the r coordinate during the negative (defocusing) pulse. For the z coordinate, formation of ions with small initial coordinates and large initial velocities is optimal (irrespective of an injection pulse). Thus, for an ion trap operating close to the

apex of the first stability zone, injection of an ionizing electron beam through the ring electrode at a right angle to the symmetry axis z is optimal. The electron beam must have the shape of a narrow sheet beam.

It should be noted that from the configuration of the ZBS in Fig. 6, it follows that base solutions of the second kind do not appear for the z coordinate because the axis $z_0 = 0$ lies out of the ZBS. At the same time, base trajectories of the first kind appear during the whole period of the rf field. For the r coordinate, on the other hand, base solutions of the first kind do not appear during the defocusing pulse, but base solutions of the second kind appear.

From the point of view of effective sorting, the use of the EC signal has good prospects for HMS [11]. The shape of the EC signal is shown in Fig. 1(b). It consists of two positive pulses separated by a time interval when the voltage is equal to zero (the active part of the EC signal), and one negative pulse. Zones of base solutions for the ion trap operated with the EC signal are shown in Fig. 7. It is seen that for the active part of the EC signal zones of base solutions on the phase plane are very small for both r and z coordinates. It follows from the conducted calculations that for the upper zones of the stability diagram (for the ion trap, for example) an ion beam must be injected during the active part of the signal.

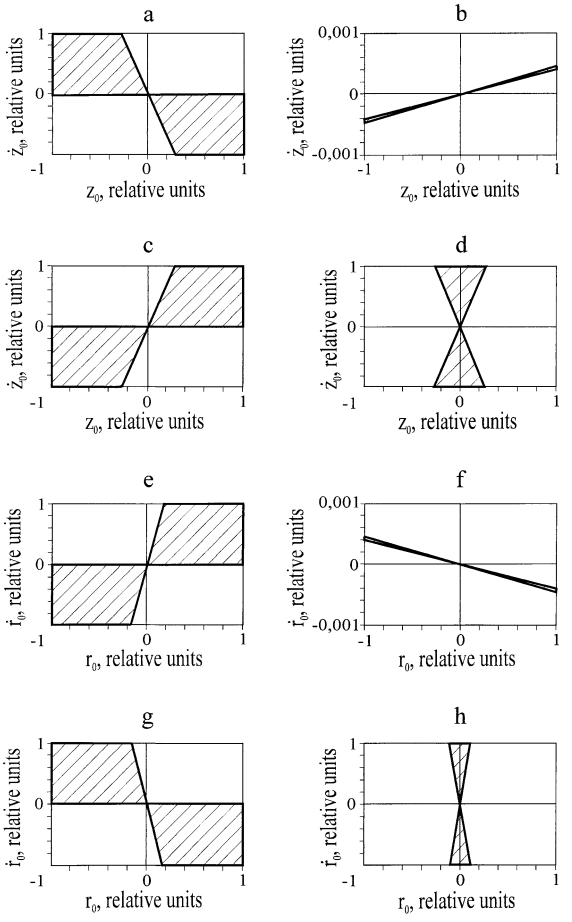

Fig. 7. Zones of base solutions for the axially symmetric ion trap in the case of the EC signal for the working points located close to the apex of the first stability zone: (a)–(d) zones of base solutions along the z coordinate: $a_2 = 4.275846$, $a_1 = 4.405942$, $\beta_{0z} = 1.005788$; (e)–(h): zones of base solutions along the r coordinate: $a_2 = 4.28498$, $a_1 = 4.415354$, $\beta_{0r} = -1.000494$; (a), (e) the first positive (focusing along the r coordinate) pulse; (b), (f) the active part of the EC signal; (c), (g) the second positive (defocusing along the r coordinate) pulse; (d), (h) the negative (defocusing along the r coordinate) pulse.

6. Influence of different factors on behavior of base trajectories and efficiency of sorting of the charged particles in HMS

We have developed a reliable computer program for mass peak calculations that considers details of base trajectories. This program allows us to investigate various factors governing base trajectories and mass peak shape. Such factors are: random fluctuations of the working signal (frequency, amplitude, dc voltage); mass scan rate and shape of a scan function; interactions of ions with molecules of the residual gas.

Calculations conducted showed that all these factors eliminate base trajectories. Trajectories are modified to conventional ones with time and tend to the steady stationary trajectories. The trapping time of unstable ions in the working volume of the HMS is decreased.

An example of the influence of fluctuations of the pulse rf voltage amplitude on a base solution is given in Fig. 8. Base trajectories in the ion trap are presented here for ideal signal (meander) without fluctuations and for a signal distorted by random fluctuations of rf voltage amplitude.

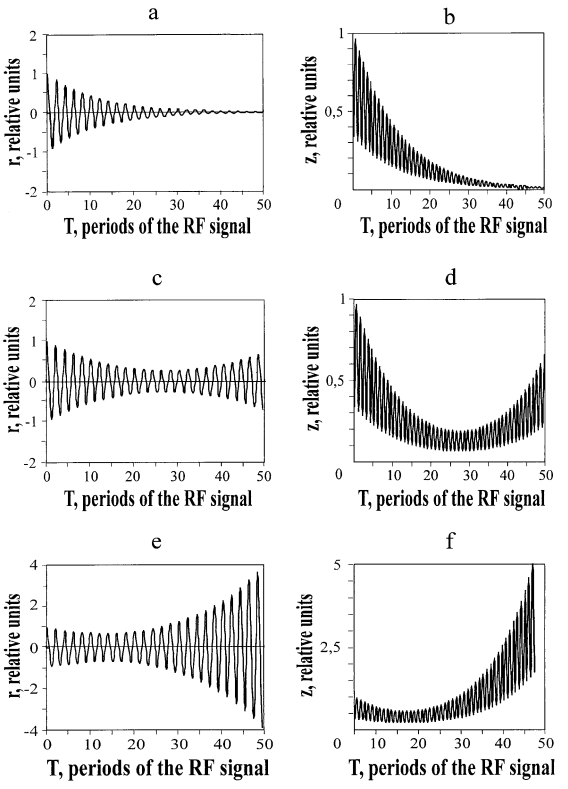

Fig. 8. Base trajectories within the axially symmetric ion trap in the case of meander: (a), (b) ideal working signal without fluctuation; (c)–(f) working signal with fluctuation of ac voltage amplitude; (c), (d) level of fluctuations is 0.01%; (e), (f) level of fluctuations is 0.1%; (c) working signal with fluctuation of ac voltage amplitude; (a), (c), (e) $a_2 = 2.509805$, $a_1 = 3.59568$, $\beta_{0r} = -1.003496$, $T_0 = 0.256783$; (b), (d), (f) $a_2 = 2.502629$, $a_1 = 3.585399$, $\beta_{0z} = 1.003666$, $T_0 = 0.258083$.

Fluctuations influence not only base trajectories but temporally converging ones that are close to the base trajectories seen in Fig. 2. When fluctuations are increased, then the "dead time" of the trajectories (a period of time when an ion coordinate is less than its initial value) is decreased. The dependence of the dead time on the "fluctuation frequency" has a minimum point at the frequency close to the basic frequency of the working signal. More destructive fluctuations for base trajectories are fluctuations of an amplitude and dc voltage of the rf signal.

Fluctuations of an rf signal shape play a positive role (there are limits, of course). It follows from the calculations that the maximum resolution can be increased up to 2–4 times by setting fluctuations for about 0.1%.

High-speed mass scans also destroy base trajectories, and decrease the demanded sorting time. An exception is a step mass scan, when a period of a step is equal to or greater than the sorting time. Numerous computer simulations of different modes of mass scanning have shown that the increasing of scan speed up to 10^3 Da s^{-1} improves the mass peak shape, and that mass scanning by changing frequency has a slight advantage.

The influence of residual gas on base trajectories can be predicted. When the concentration of a light buffer gas in the ion trap is increased, the dead time of the base trajectories and trajectories close to the base ones is decreased and the efficiency of sorting unstable ions is increased.

7. Experimental

It follows from the conducted computer simulation that the negative influence of the base trajectories on charged particle analysis and the mass peak shape depends on features of charged particle injection into the rf field and the shape of the working rf signal. In order to improve the mass peak shape it is preferable to inject the electron beam during the negative (defocusing along the r axis) pulse when the ion trap operates with the meander [Fig. 1(a)]. The use of the EC signal [Fig. 1(b)] yields the better mass peak shape. These results encouraged us to experimentally compare mass peak shapes obtained with signals of both types.

Experiments were carried out on the axially symmetric ion trap with characteristic dimensions $d = 19$ mm and $r_a = 19$ mm, operated in the upper apex of the first stability zone. The ionizing electron beam was injected in a radial plane through the narrow radial slit (0.3×10 mm) in the ring electrode. A nominal electron energy of 70 eV was kept constant. It was possible to inject the electron beam during any phase of the rf signal. The working pressure was about 2×10^{-6} Torr.

Timing sequences for the operation of the ion trap in the experiments are shown in Fig. 9. When the ion

trap operated with the meander [Fig. 9(a)], a positive dc potential of (156–162) V was applied to the ring electrode, and an rf pulse of positive polarity with amplitude of 240 V was applied to the endcap electrodes. The duration of the positive pulse was equal to the duration of the interval with zero potential. The voltage stability was about 10^{-4}.

To form the EC signal [Fig. 9(b)] we used two rf pulse signals. The first rf signal of positive polarity with amplitude of (235–255) V was applied to the ring electrode. The second rf signal of positive polarity with amplitude of 220 V was applied to the endcap electrodes. Thus, two positive pulses with equal duration (separated by a time interval when the voltage is equal to zero) and one negative pulse make one period of the EC signal. A mass scan was performed by changing the frequency of both rf signals. The rf signals (meander and the EC signal) were formed by the same output stages of a pulse generator.

Each sorting cycle started from ionization (during one period of the rf signal, t_p) when the potential of the filament was set to the value that provided the required ionization energy (Fig. 9, OA). The potential of the filament was maintained positive in order to cut off the electron beam during the ion sorting. At the end of a preset sorting time (Fig. 9, AB), the potential of electrodes was changed and the sorted ions were ejected through a shaped grid in one of the endcaps (a constant positive potential was applied to the ring electrode in the case of the EC signal, and the potential of the endcap electrode was equal to zero in the case of the meander), Fig. 9, BC.

8. Results and discussion

Mass peaks of *m/z* 28 obtained for ionization during the positive (focusing along the *r* coordinate) and the negative (defocusing along the *r* coordinate) pulses of the meander are shown in Fig. 10. Intensity of the peaks was normalized to the maximum peak height. Experiments were done for a sorting time of 70 rf periods and for one position of working line on the stability diagram. We can see from Fig. 10 that the electron beam injection during the defocusing pulse gives a mass peak with sharper edges (mass peak 2). This indicates that the sorting efficiency in this case is much higher. In the unstable region for the *z* coordinate (this corresponds to the higher masses or to the right edge of the peak) the sorting efficiency for the "unstable" ions differs slightly. In the unstable region for the *r* coordinate (this corresponds to the lower masses or to the left edge of the peak) the sorting efficiency changes significantly. These experimental results match the results of theoretical calculations presented in Fig. 6. Furthermore, the maximum resolution is more than two times greater, and resolution was increased with an increase of the sorting time.

Mass peaks of *m/z* 28 obtained for the EC signal and the sorting time $n_{\text{sort}} = 70$ periods are demonstrated in Fig. 11. The electron beam was injected during the first positive pulse (mass peak 1) and the active part of the rf signal (mass peak 2). The sorting efficiency was much higher when ionization was carried out during the active part of the period. The maximum resolution, obtained for the greater slope of the working line, is three times greater than for injection during the first focusing pulse.

In Fig. 12 we compare mass peaks of *m/z* 28 achieved with the ion trap, operated with a pulse signal (meander) and the EC signal. Mass peak 1 in this figure corresponds to ionization during the negative (defocusing) pulse of the meander, and mass peak 2 corresponds to ionization during the active part of the EC signal. The experiments were done with a sorting time of 90 periods of the rf field. The use of the EC signal improves the peak shape. More impressive results have been achieved when we compared maximum resolutions defined at the different levels of the peak maximum. For meander we had a resolution of 120 at a level of 10^{-1} that falls down to a resolution of about 30 at a level of 10^{-5}. At the same time, for the EC signal a resolution of 300 was achieved at a level of 10^{-1} and 220 at a level of 10^{-5}. Computer simulations of mass peaks in terms of base trajectories, conducted in our laboratory, completely match these experimental results.

We compare mass peaks by estimation of the

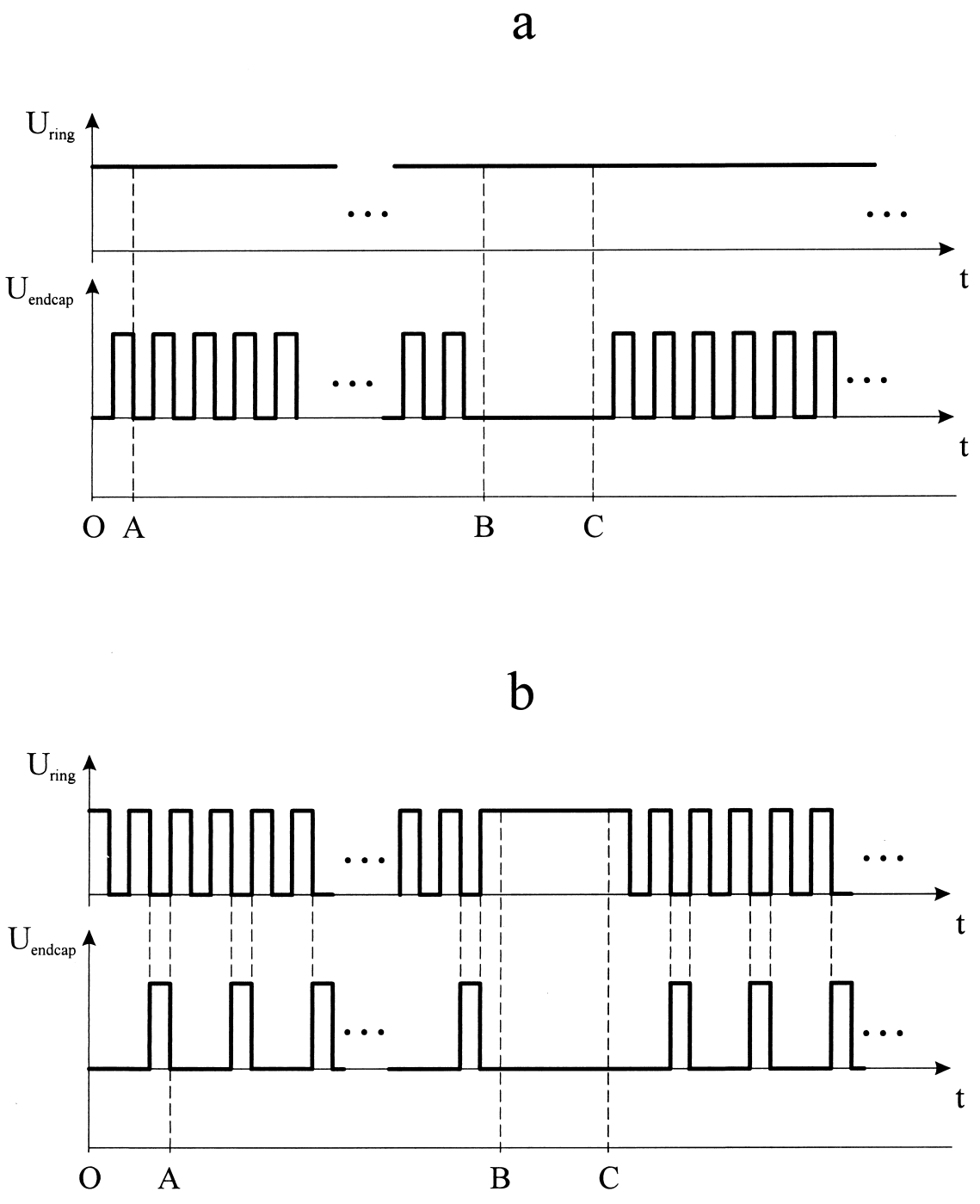

Fig. 9. Timing sequences for operation of the ion trap in the experimental studies of the mass peak shape: (a) meander; (b) EC signal; U_{ring} is the potential of the ring electrode; U_{endcap} is the potential of the endcap electrodes; OA—ionization; AB—ion sorting; BC—ion ejection; OC—a working cycle.

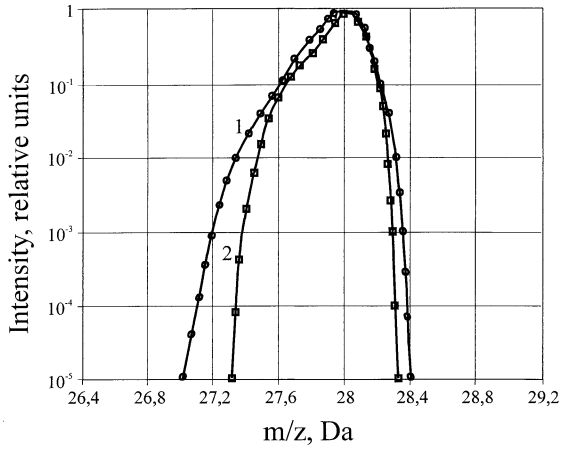

Fig. 10. Mass peak shapes obtained in experiments with the ion trap for 70 sorting periods; working signal is meander; 1—the ionizing electron beam was injected during the positive pulse (focusing along the *r* coordinate); 2—ionization during the negative pulse (defocusing along the *r* coordinate).

quotient of resolution defined at the levels of the peak maximum differing by an order of 10:

$$K_f = R_{10L}/R_L$$

where L is a level at which resolution is defined. Let us call this parameter a coefficient of a peak shape. The values of this coefficient, averaged over several

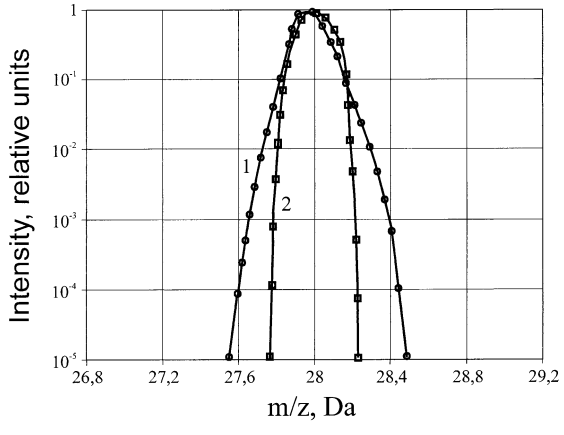

Fig. 11. Mass peak shapes obtained in experiments with the ion trap for 70 sorting periods; working signal is EC signal; the first stability zone; 1—the ionizing electron beam was injected during the first positive pulse (focusing along the *r* coordinate); 2—ionization during the active part of the EC signal.

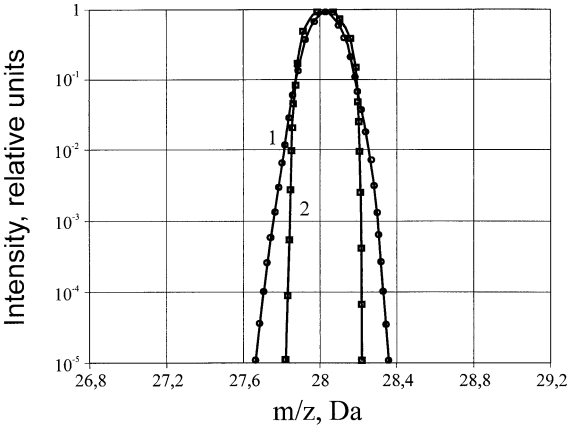

Fig. 12. Mass peak shapes obtained in experiments with the ion trap operated in the first stability zone for 90 sorting periods; 1—the working signal is meander; the ionizing electron beam was injected during the negative pulse (defocusing along the *r* coordinate); 2—the working signal is EC signal; the ionizing electron beam was injected during the active part of the signal.

levels (beginning from the level 10^{-1}) for the meander and the EC signal are presented in Table 1. It can be seen from this table that the theory corresponds to experimental data, and that use of the EC signal is preferable to the meander.

9. Conclusions

The results presented in this article were unexpected, even for the authors. We chose to submit our article for this special issue thanks to professor Raymond E. March's idea [12] that: "The theory of ion trap operation differs from those of other mass

Table 1
The values of coefficients of a peak shape K_f for different signal types

Type of signal		K_f 70 periods of sorting	K_f 90 periods of sorting
Meander	Experiment	1.480	1.475
	Theory	1.530	1.450
EC signal	Experiment	1.111	1.091
	Theory	1.109	1.070

spectrometers and presents an exciting challenge to the mass spectrometry community."

We did not consider the practical aspects of base trajectories for HMS. But, we do hope that attempts will be made to develop instruments with high analytical parameters utilizing remarkable properties of converging trajectories of ions (base trajectories).

References

[1] W. Paul, H. Steinwedel, German Patent 944,900 (1956); US Patent 2,939,952 (1960).
[2] W. Paul, H.P. Reinhard, U. von Zahn, Zeitschrift fur Physik 152 (1958) 143.
[3] P.H. Dawson, N.R. Whetten, Adv. Electron. Electron Phys. 27 (1969) 59.
[4] P.H. Dawson, Quadrupole Mass Spectrometry and Its Applications, Elsevier, Amsterdam, 1976.
[5] R.E. March, R.J. Hughes, J.F.J. Todd, Quadrupole Ion Storage Mass Spectrometry, Wiley Interscience, New York, 1989.
[6] J.F.J. Todd, Mass Spectrom. Rev. 10 (1991) 3.
[7] R.E. March, J.F.J. Todd (Eds.), Practical Aspects of Ion Trap Mass Spectrometry, CRC, Boca Raton, FL, 1995, Vols 1, 2, and 3.
[8] N.W. McLachlan, Theory and Applications of Mathieu Functions, Clarendon, Oxford, 1947.
[9] E.P. Sheretov, W.I. Terentiev, J. Tech. Phys. 42(5) (1972) 953.
[10] E.P. Sheretov, B.I. Kolotilin, J. Tech. Phys. 42(9) (1972) 1931.
[11] E.P. Sheretov, B.I. Kolotilin, A.V. Brykov, Proceedings of the 14th International Mass Spectrometry Conference, Tampere, Finland, August, 1997, p. 229.
[12] R.E. March, J. Mass Spectrom. 32 (1997) 351.